THE ATOMISTIC STUDY ON THERMAL TRANSPORT OF THE BRANCHED CNT

Wei-Jen Chen **I-Ling Chang***

Department of Mechanical Engineering
National Cheng Kung University
Tainan, Taiwan

ABSTRACT

In this research, the thermal transport behavior of the branched carbon nanotube (CNT) with T-junction was investigated using non-equilibrium molecular dynamics simulation. Both symmetric and asymmetric temperature-controlled simulations were imposed to evaluate how the heat flowed inside the branched CNT with three branches of equal length and same chirality. The branch length and strain effects on the heat flow were examined. In addition, the simulated heat flow was compared with the prediction made by conventional thermal circuit calculation based on diffusive phonon transport. The heat was observed to flow straight rather than sideway inside the branched CNT with T-junction under the asymmetric temperature setup; this finding contradicts the conventional thermal circuit calculation. There are two possible explanations for this phenomenon. One is ballistic phonon transport and the other is phonons have different interactions or scattering with the defective atomic configurations at the T-junction. Moreover, the tensile strain could tune the heat flow, a finding that might be useful in thermal management applications.

Keywords: ballistic, diffusive, branched CNT, heat transfer

1. INTRODUCTION

For decades, the size of electronic devices has decreased from few microns to nanometers, and the thermal management of these nanoelectronic devices has become a severe challenge to ensuring high performance and reliability. Materials with high thermal conductivity are required to effectively dissipate thermal energy. Carbon nanotubes and their derivate structures are the most promising building blocks for thermal management applications because of their high thermal conductivity and stable mechanical properties [1, 2]. Single-walled or multi-walled CNTs are quasi-one dimensional structures, and thermal conduction is limited to one direction. To efficiently transfer energy in all the desired directions, several nanotube structures (e.g., CNT bundles [3, 4], pillared graphene [5-7], branched CNTs with X-, T-, Y- [8, 9] or intermolecular junctions [10-12], and CNT networks [11, 13]) have been proposed for different purposes. Among these structures, branched CNTs are of special interest for their potential to rectify electric current [14-16] or heat [8, 17]. It would be important to study the thermal transfer behavior inside the branched CNTs for their future application.

Recently, branched CNTs have been synthesized in high quality, purity, and even at low cost using various approaches (e.g., aerosol technique [14, 15], controlled catalysts by chemical vapor deposition [16, 18, 19], and forming molecular junctions by electron beam welding [20, 21]). However, only few literatures have reported on the thermal conduction measurement of the branched CNTs, probably because of their complicated geometry and nanometer size. The experimental measurement is difficult but technically possible. Moreover, thermal transport inside these nanostructures could not simply be explained by diffusive based heat conduction equation because the phonon mean path is compatible or larger than the structural characteristic size. Some researchers have attempted to investigate the thermal transfer behavior inside branched CNTs using molecular dynamics simulation, which is an appropriate tool to characterize the atomic collective and individual behaviors at nanoscale. Noya et al. [8] demonstrated the existence of thermal rectification by imposing heat pulse on the stem or branches of Y-junction CNT and the heat pulse was found to propagate unimpeded from stem to branches, whereas in the reverse direction, a substantial reflection with significantly reduced transmission was observed. Li et al. [22] investigated the temperature dependence of thermal rectification in Y-junction CNT. Park et al. [9] imposed wave packet on branched CNTs with T- and X-junction and observed the energy transmission, ramification and reflection ratios on branches for the longitudinal acoustic, twisting, transverse acoustic, radial breathing, and flexural optical modes. They discovered that both the nanotube diameter and the junction type

* Corresponding author (ilchang@mail.ncku.edu.tw)

DOI : 10.1017/jmech.2020.37

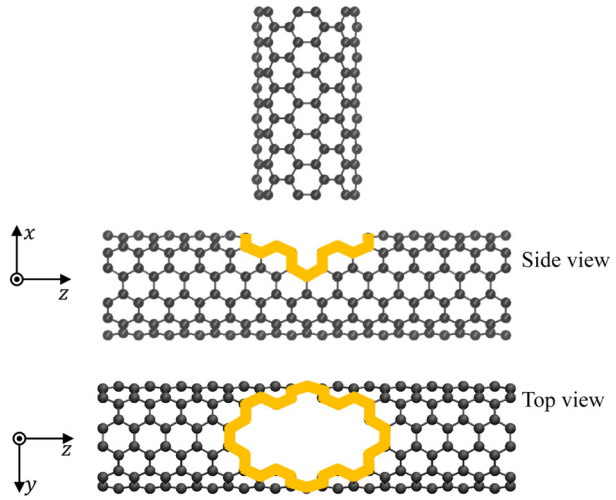

Fig. 1. Illustration of the branched CNT before thermal welding.

would affect phonon scattering, and thus influence the transmission of vibrational energy.

However, heat pulse could account for transient thermal phenomena while wave packet simulation could only provide phonon information at 0 K. In heat pulse simulation, the leading edge transport phenomenon is determined by the nature and propagation of discrete phonon modes and not included the long-time contributions from the possible diffusive components. The wave packet simulation does not include the phonon-phonon scattering and could not give physical insights on overall heat flow inside the branched CNTs. To the best of our knowledge, no previous reports have examined the stable heat flow behavior inside the branched CNT. In this paper, the heat flow inside the branched CNT with T-junction will be investigated using nonequilibrium molecular dynamics (NEMD) simulation. The T-junction was constructed by the thermal welding of two pre-designed nanotubes and three branches of same chirality and length are attached to the T-junction. Both symmetric and asymmetric temperature-controlled simulations were performed to study the heat flow. The branch length and strain effects at the T-junction on the heat flow inside the branched CNTs were also studied.

2. METHODOLOGY

The thermal transport behavior of the branched CNT with T-junction was investigated using NEMD simulation. Both symmetric and asymmetric temperature setups were applied on three identical branches to study the heat flow. The branch length and strain effects on the heat flow in the branched CNT were examined.

The CNT T-junction was created by thermal welding method as proposed in the literature [20]; some atoms were removed manually from one pristine (6,6) nanotube of 4nm to create defects in the crossing region as illustrated in Fig. 1. The atoms must be removed in a way to satisfy the topological requirement described by

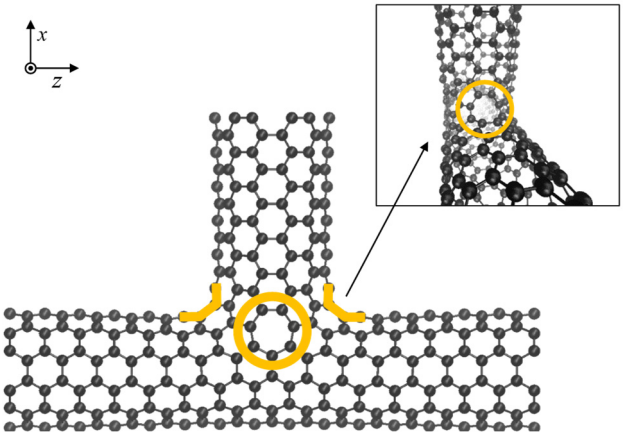

Fig. 2. Atomic configuration of the T-junction part.

Euler equation [23], where the numbers of pentagons (n_5), heptagons (n_7) and octagons (n_8) follow the relation, $2n_8 + n_7 - n_5 = 6$. Another 1.5-nm (6,6) CNT was placed vertically above the crossing region of the defected CNT. Subsequently, these two nanotubes were moved closer and simultaneously heated up to 4000K to perform the thermal welding. The high temperature was adopted in order to accelerate the creation of interlinks and surface reconstruction. Subsequently, the T-junction model is cooled down to 300K. Adaptive intermolecular reactive bond order (AIREBO) potential [24] was employed throughout this research to describe the interatomic interaction of carbon atoms. The time step is 1 fs. By systematically removing the carbon atoms, the topological defects at the junction area can be quantitatively controlled. Two heptagon rings (one in the backside) and two octagons were observed at the corner region of the T-junction as illustrated in Fig. 2. It is worth to mention that it is possible to construct other T-junctions with different defects (i.e., pentagons, heptagons and octagons) by removing designed atoms at the connecting part, as long as the topological requirement are satisfied.

The branched CNT was created by connecting three (6,6) nanotubes of equal lengths to the T-junction part. To investigate the effect of the branch length on the heat flow inside the branched CNT, various branch lengths of 25–200 nm were simulated and the whole system was relaxed using canonical (NVT) ensemble under 300K at the T-junction. To release the stress inside the branched CNT, the atoms on each individual branch were allowed to move only along its axial direction under microcanonical (NVE) ensemble, and the equilibrating process is run for 1 ns. Through this relaxation procedure, both the longitudinal and transverse stresses inside the branches could be eliminated. It was essential to relax the structure because the residual stress from the initial model could influence the material properties, thus affecting the heat flow.

Both symmetric and asymmetric temperature setups, as displayed in Fig. 3(a) and (b), were imposed on the branched CNT to investigate the heat flow inside the branches using NEMD simulation. In order to avoid rigid body motion (i.e., translational movement and

https://doi.org/10.1017/jmech.2020.37 Published online by Cambridge University Press

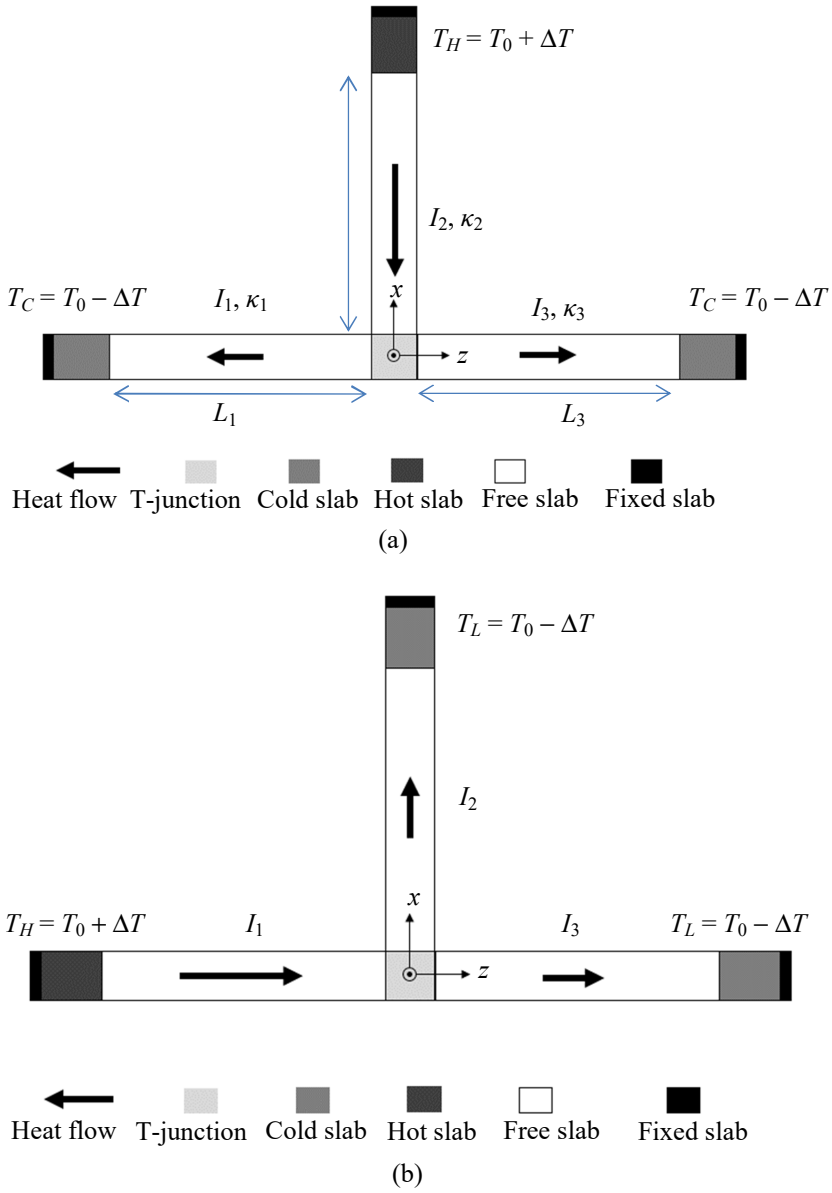

Fig. 3. Illustration of two temperature-controlled NEMD, (a) symmetric and (b) asymmetric setup. The length, L; heat current, I; and thermal conductivity, κ; of each branch are marked in the figure.

rotation) of the branched CNT, three branches were fixed at the end for 0.5 nm near the 5-nm temperature controlled region. The temperatures in the hot and cold regions are controlled at 300 ± 300K using Langevin thermostat. NVE ensemble was imposed on the free area of the branched CNT for 1 ns to reach steady state; the results were averaged at the following 1 ns. Each model was simulated and averaged for six times with different initial velocities.

In the symmetric temperature setup, heat current flowed from vertical branch (branch 2) to the two horizontal ones (branch 1 and 3). To investigate the heat flow inside the branched CNT, the heat current ratio after junction separation was defined as follows:

$$R_1 = \frac{I_1}{I_1 + I_3} \times 100\% \; ; \; R_3 = 1 - R_1 \tag{1}$$

where $I_{1(3)}$ is the power taken out from the temperature controlled region of branch 1(3). For asymmetric temperature-controlled simulation, heat current will flow from one horizontal branch (branch 1) to the other horizontal one (branch 3) and vertical one (branch 2). The heat current ratio after junction separation is defined in similar manner as follows:

$$R_2 = \frac{I_2}{I_2 + I_3} \times 100\% \; ; \; R_3 = 1 - R_1 \tag{2}$$

Moreover, tensile strain was applied on the horizontal nanotube to examine the effect of strain on the heat flow inside the branched CNT. Only the tensile strain effect was studied because the CNT is a slender structure susceptible to structural instability (i.e., buckling) under compression.

https://doi.org/10.1017/jmech.2020.37 Published online by Cambridge University Press

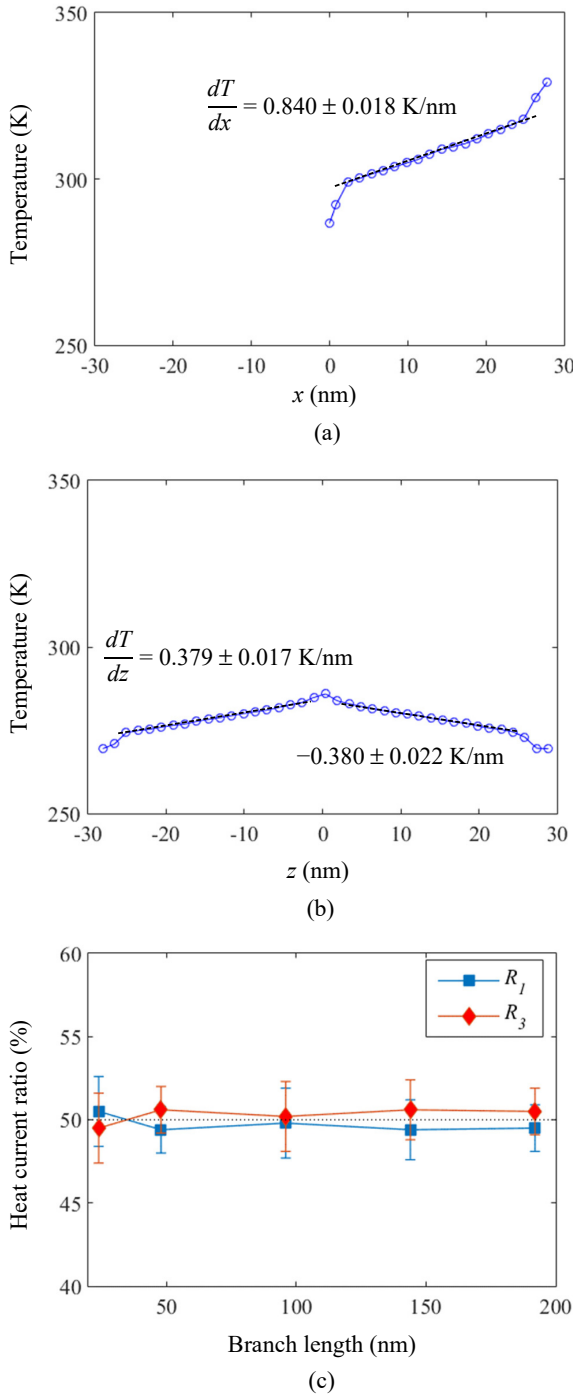

Fig. 4. Under symmetric temperature-controlled NEMD simulation, the steady-state temperature profile of (a) the vertical branch and (b) horizontal one for the branched CNT with 25nm branch length, and (c) the heat flow for various branch lengths.

3. RESULTS

Under the symmetric temperature setup, the steady-state temperature profile was obtained by calculating the atomic kinetic energy inside each slab for last 1 ns. Each slab contains the same number of atoms even at the T-junction part. The steady-state temperature profile for the branched CNT with 25 nm branch length and the heat flow inside the branched CNT for various branch lengths are illustrated in Fig. 4(a)–(c). Nonlinear temperature regions were observed near the T-junction part and temperature-controlled regions because of the strong phonon scattering effect caused by the mismatching of the lattice-vibrational spectra [25]. It is observed that the temperature gradients are approximately the same, within 0.5% difference, at the two horizontal branches (branch 1 and 3), and the heat currents were near equal, regardless of the branch length. The equal heat flow into two branches is predictable because the geometry and chirality of the two branches are the same, and the atomic configuration at the T-junction part is also symmetric with respect to the heat flow direction. The result also agrees with the prediction by conventional thermal circuit using the same thermal conductivity for each branch ($k_1 = k_2 = k_3$) and branch length ($L_1 = L_2 = L_3$) as illustrated in Fig 3(a).

Under asymmetric temperature setup, the temperature profile for the branched CNT with 25 nm branch length and the heat flow inside the branched CNT for various branch lengths are illustrated in Fig. 5(a)–(c). Similar nonlinear temperature regions to those in symmetric temperature case were noted. Both the linear temperature gradients and heat currents at branch 2 and 3 differed consistently within 10-20%, from which the thermal conductivities could be computed based on Fourier's law. It was found that the thermal conductivities of branch 2 and 3 were close within error to each other for various branch lengths. Besides, it is noticed that, from Fig. 5(c), heat did not flow equally into the two branches after the junction separation. Instead, heat current flowed preferentially straight to the horizontal branch rather than sideway (i.e., $R_3 > 50\%$ or $R_2 < 50\%$). However, as the branch length increased to 200nm, the heat current ratio of branch 2 tended to approach 50%. According to the diffusive based conventional thermal circuit calculation, the heat current ratio should remain at 50% because the two branches are identical.

There are two postulates to explain the contradiction between the simulation results and the prediction: 1. The heat was transported in ballistic way, instead of diffusively scattering inside the short branch. When the branch length was longer than the phonon mean free path (i.e., 0.5 – 1.5 μm) [26], there were ballistic to diffusive crossover of heat flow and the heat will be transported more by diffusively scattering. 2. Phonons exhibited different interactions or scattering with defective atomic configurations (i.e., heptagonal and octagonal rings) at T-junction part. Hence, T-junction has directional effect on heat current. This became more obvious in asymmetric temperature simulation of branched CNT since the thermal conductivities of the two branches were calculated to be approximately the same irrespective to branch length. However, this T-junction directional effect became less significant when the branch length becomes longer because thermal resistance came more from the branches than from the T-junction. Both postulates appear reasonable to explain the simulation results, but further research is required to investigate which one is correct.

https://doi.org/10.1017/jmech.2020.37 Published online by Cambridge University Press

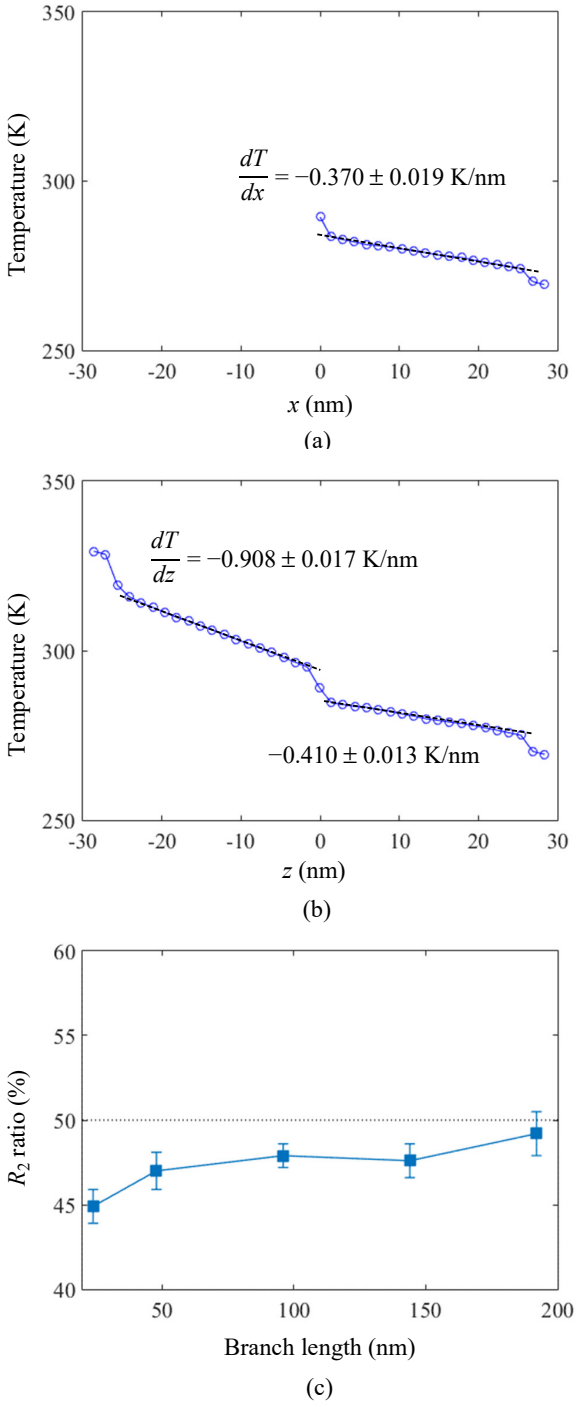

Fig. 5. Under asymmetric temperature-controlled NEMD simulation, the steady state temperature profile of (a) the vertical branch and (b) the horizontal one for the branched CNT with 25-nm branch length, and (c) the heat flow inside the branched CNT for various branch lengths.

At each time step, the energies added or removed from the thermal baths (hot and cold controlled regions) in all three branches were recorded. As depicted in Fig. 6, the total power taken out from the cold regions and pumped into the hot one was almost the same, which means the total energy is conserved in the system for both symmetric and asymmetric temperature setups. However, it is

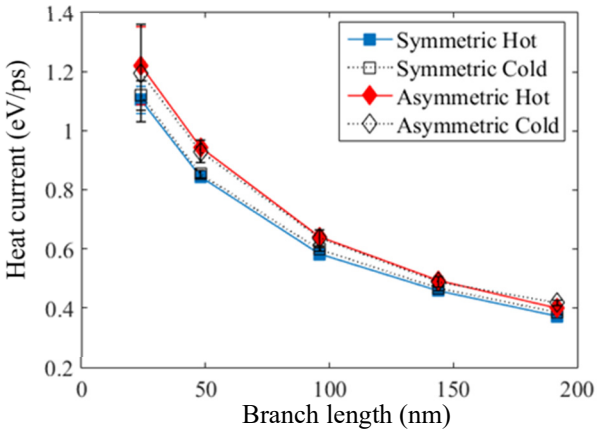

Fig. 6. Power supplied or taken from thermal baths for the branched CNT with various branch lengths under symmetric and asymmetric temperature setups.

interesting to notice that the total power for asymmetric temperature setup was always higher than the symmetric setup; this indicates that thermal rectification can be achieved by merely switching the high and cold temperature regions. In addition, the power differences between the two temperature setups became smaller as the branch length increase; this could also be explained by the two postulates. The thermal rectification behavior is similar to heat pulse simulation of Y-junction with stem and branch in the literature [8, 22] but it is not easy to make comparison on the rectification effect. From ballistic phonon transport point of view, there would be shorter phonon-boundary or phonon-defect path for symmetric temperature setup because all the phonons were forced to change propagating directions through interactions with the boundaries or defects at T-junction. Thus, the thermal resistance for symmetric temperature setup would be higher than asymmetric temperature setup. As for how the phonons interact or scatter with the defective atomic configurations at T-junction, more research is needed in order to fully unveil the mechanism.

Finally, the effect of strain on the stable heat flow inside the branched CNT was investigated. Under the symmetric temperature-controlled simulation, the tensile strain applied on the horizontal nanotube exerted no noticeable effect on the heat flow. The heat still flowed equally to two horizontal branches. However, the tensile strain had noticeable effect on the heat flow inside the branched CNT for the asymmetric temperature-controlled simulation as illustrated in Fig. 7. With the assistance of small tensile strain, more heat flow straight to branch 3. However, a larger tensile strain will even made heat flow more into branch 2 for both branch length of 25 and 100nm. This result indicates that it is possible to tune the heat flow by applying tensile strain.

We attempted to investigate the tensile strain dependence of the thermal conductivities of pristine (6,6) CNT using nonequilibrium molecular dynamics simulation. Two lengths, 50 nm and 200 nm, of pristine CNT were simulated since they were corresponding to the total length

https://doi.org/10.1017/jmech.2020.37 Published online by Cambridge University Press

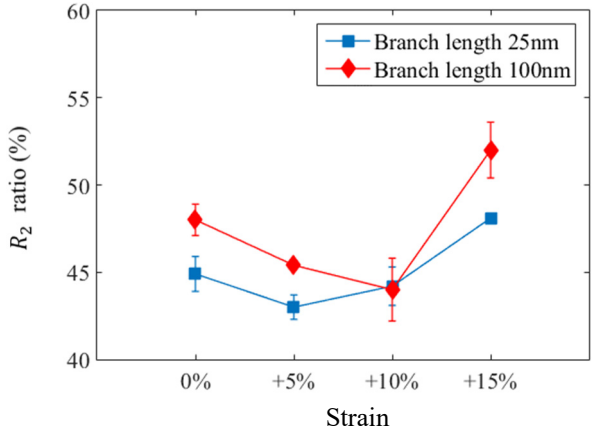

Fig. 7. Strain effect on the heat flow inside the branched CNT under the asymmetric temperature setup for two different branch lengths.

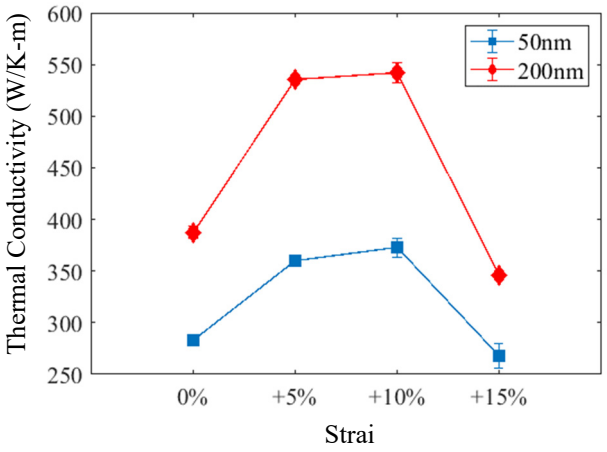

Fig. 8. Strain effect on the thermal conductivity of the pristine CNT with length of 50nm and 200nm.

of the horizontal branches (branch 1 and 3) considered in Fig. 7. The CNT was fixed at two ends and temperatures controlled regions of 5nm length were set next to the fixed region. The temperatures in the hot and cold regions were controlled at $300 \pm 30K$ using Langevin thermostat. The thermal conductivity, k, of the pristine CNT could be obtained from simulation by Fourier's law as

$$\kappa = -\frac{J_z}{\partial T / \partial z} \tag{3}$$

where $\langle J_z \rangle$ is the heat current and $\langle \partial T / \partial z \rangle$ is the temperature gradient along the axial direction of CNT. After reaching steady state, we can obtain heat current as

$$\langle J_z \rangle = \frac{\Delta \varepsilon}{t_s A_c} \tag{4}$$

where t_s is the time after the simulation reaches steady state, $\Delta\varepsilon$ is the accumulative kinetic energy which added or removed from thermostat slabs, and A_c is the cross-section area of the system. For CNT, the cross-section area can be calculated as $A_c = \pi D_c b$, where b is the thickness of nanotube wall and D_c is the diameter. The CNT diameter can be computed by $D_c = \frac{a_{c-c}\sqrt{3\times\left(n^2+m^2+nm\right)}}{\pi}$, where a_{c-c} is the length of carbon-carbon bond (1.418 Å), and the interlayer distance (3.4 Å) between graphite sheets is used as the wall thickness. The temperature gradient of system can be obtained from the linear region at temperature profile.

As illustrated in Fig. 8, we found that the thermal conductivity would increase first as tensile strain increases up to 10%; as strain increases further to 15%, the thermal conductivity would decrease. This trend was consistent with the axial stress results published by Ren et al. [27]. It is worth to mention that the thermal conductivities of the pristine CNTs obtained in our simulation were similar to those in the literature [28, 29]. Meanwhile, the thermal conductivity of the vertical branch (branch 2) would not be affected by the applied strain on the horizontal branches. This could be used as a crude explanation for the strain dependence of the heat current ratio in branch 2, R_2, under asymmetric temperature setup. However, the underlying mechanism for the strain dependence of the heat current ratio inside the branched CNT needs further investigation. It would involve how the strain influences ballistic phonon transport and phonon-defect interaction at T-junction.

4. CONCLUSIONS

NEMD simulation was employed to study the thermal transport behavior inside the branched CNT with T-junction. The T-junction part was prepared by the thermal welding of two (6,6) CNTs with atoms removed in a way to satisfy the topological requirement. Heptagonal and octagonal rings existed in the T-junction part and the three connecting branches were of the same length and chirality. Two temperature-controlled simulations, namely symmetric and asymmetric, were performed to investigate the heat flow inside the branched CNT. For the symmetric temperature setup, heat flowed equally into the two horizontal branches, irrespective of the branch length, as predicted by the conventional thermal circuit calculation. As for the asymmetric temperature setup, heat preferred to flow straight rather than sideway in branched CNT, especially for shorter branch length. There are two possible explanations for that phenomenon. One is ballistic phonon transport, and the other is that phonons exhibit different interactions or scattering with the defective atomic configurations (i.e., heptagons and octagons) at T-junction. Moreover, it was found that the tensile strain applied on the horizontal nanotube could tune the heat current ratio, a finding that might be useful in thermal management applications.

https://doi.org/10.1017/jmech.2020.37 Published online by Cambridge University Press

ACKNOWLEDGEMENTS

This research work was financially supported by the Taiwan Ministry of Science and Technology under the grants MOST 106-2923-E-006-004-MY3 and MOST 105-2628-E-006-003-MY3. The authors also want to thank Mr. Yu-Wei Lo for preparing the T-junction model.

REFERENCES

1. Berber, S., Kwon, Y. K. and Tománek, D., *Physical Review Letters*, **84**, pp. 4613 (2000).
2. Ruoff, R. S. and Lorents, D. C., *Carbon*, **33**, pp. 925 (1995).
3. Vollebregt, S.et al., *Journal of Applied Physics*, **116**, pp. 023514 (2014).
4. Gharib-Zahedi, M. R., Tafazzoli, M., Bohm, M. C. and Alaghemandi, M., *The Journal of Chemical Physics*, **139**, pp. 184704 (2013).
5. Park, J. and Prakash, V., *Journal of Materials Research*, **28**, pp. 940 (2012).
6. Shi, J., Dong, Y., Fisher, T. and Ruan, X., *Journal of Applied Physics*, **118**, pp. 044302 (2015).
7. Shi, J., Zhong, Y., Fisher, T. S. and Ruan, X., *ACS Applied Materials & Interfaces*, **10**, pp. 15226 (2018).
8. Gonzalez Noya, E., Srivastava, D. and Menon, M., *Physical Review B*, **79**, pp. 115432 (2009).
9. Park, J., Lee, J. and Prakash, V., Journal of Nanoparticle Research, 17, pp. 59 (2015).
10. Alaghemandi, M., Muller-Plathe, F. and Bohm, M. C., *Journal of Chemical Physics*, **135**, pp. 184905 (2011).
11. Chen, J. et al., *ACS Applied Materials & Interfaces*, **4**, pp. 81 (2012).
12. Aitkaliyeva, A., Chen, D. and Shao. L., *Scientific Reports*, **3**, pp. 2774 (2013).
13. Lian, F., Llinas, J. P., Li, Z., Estrada, D. and Pop, E., *Applied Physics Letters*, **108**, pp. 103101 (2016).
14. Kaskela, A. et al., *Nano Letters*, **10**, pp. 4349 (2010).
15. Sun, D. M. et al., *Nature Nanotechnology*, **6**, pp. 156 (2011).
16. Hu, J., Ouyang, M., Yang, P. and Lieber, C. M., *Nature*, **399**, pp. 399 (1999).
17. Aiyiti, A. et al., *Carbon*, **140**, pp. 673 (2018).
18. Li, Y.-L., Kinloch, I. A. and Windle, A. H., *Science China Technological Sciences*, **304**, pp. 276 (2004).
19. Ma, X. and Wang, E. G., *Applied Physics Letters*, **78**, pp. 4 (2001).
20. Terrones, M., Banhart, F., Grobert, N., Charlier, J. C., Terrones, H. and Ajayan, P., *Physical Review Letters*, **89**, pp. 075505 (2002).
21. Srivastava, D., Menon, M. and Ajayan, P. M., *Journal of Nanoparticle Research*, **5**, pp. 395 (2003).
22. Li, W., Fong, Y., Tong, Z. and Zhang, S., *Acta Physica Sinica*, **62**, pp. 076107 (2013).
23. Zhang, Z., Kutana, A., Roy, A. and Yakobson, B. I., *The Journal of Physical Chemistry C*, **121**, pp. 1257 (2017).
24. Stuart, S. J., Tutein, A. B. and Harrison, J. A., *Journal of Chemical Physics*, **112**, pp. 6472 (2000).
25. Shiomi, J. and Maruyama, S., *Japanese Journal of Applied Physics*, **47**, pp. 2005 (2008).
26. Hone, J., Whitney, M., Piskoti, C. and Zettl, A., *Physical Review B*, **59**, pp. R2514 (1999).
27. Ren, C., Zhang, W., Xu, Z., Zhu, Z. and Huai, P., *The Journal of Physical Chemistry C*, **114**, pp. 5786-5791 (2010).
28. Marconnet, A. M., Panzer, M. A. and Goodson, K. E., *Reviews of Modern Physics*, **85**, pp. 1295-1326 (2013).
29. Zhang, K., Fan, H. and Yuen, M. M. F., Proceedings of the International Conference on Electronic Materials and Packaging, pp. 1-4 (2006).

(Manuscript received January 15, 2020,
accepted for publication May 01, 2020.)